Tuning the Linkers in Polymer-Based Cathodes to Realize High Sulfur Content and High-Performance Potassium−Sulfur Batteries

Published as part of The Journal of Physical Chemistry virtual special issue "125 Years of The Journal of Physical Chemistry".

Leiqian Zhang, Lingfeng Ge, Guanjie He, Zhihong Tian, Jiajia Huang,* Jingtao Wang, Dan J.L. Brett, Johan Hofkens, Feili Lai,* and Tianxi Liu

Read Online

ACCESS | Metrics & More | Article Recommendations | SI Supporting Information

ABSTRACT: The development of effective rechargeable potassium−sulfur (K−S) batteries has been retarded by a severe polysulfide shuttle effect and low sulfur content in the cathode (generally less than 40 wt %). Herein, a series of sulfur-linked polymers with different numbers of allyloxy linkers have been chosen to explore their effect on the performance of K−S batteries. By taking sulfur-linked tetra(allyloxy)-1,4-benzoquinone polymer (poly(S4-TABQ)) as the cathode of K−S batteries, its maximal sulfur content reaches ∼71 wt %, which displays a high capacity retention of 94.5% after 200 cycles (only 0.027% loss per cycle). Theoretical analyses and density functional theory calculations show that the abundant allyloxy linkers in poly(S4-TABQ) cathodes play a vital role in inhibiting the polysulfide shuttle effect and realizing high capacity, owing to the strong interaction of the allyloxy moieties with potassium polysulfides and the accelerated charge transfer during charge/discharge process. Moreover, ex situ X-ray photoelectron spectroscopy and ultraviolet−visible spectroscopy analysis are conducted to explore the electrochemical mechanism in poly(S4-TABQ) cathodes, indicating that $-C\text{-}S_n^-\cdot K^+$ (n = 2−6) and K_2S_n (n = 2−6) coexist in K−S batteries without the formation of K_2S groups. This study provides a novel insight into the application of sulfur-linked polymers as cathode material in potassium−sulfur batteries.
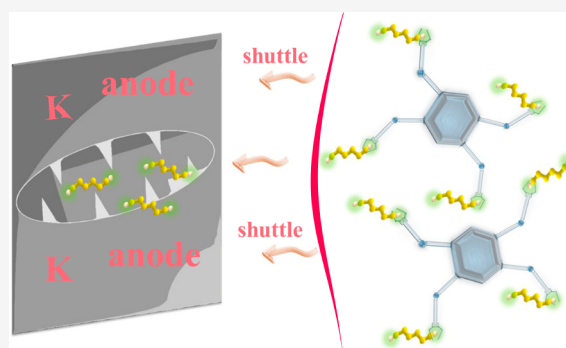
1. INTRODUCTION

As one of the most successful modern energy storage systems, lithium-ion batteries hold a dominant position in the market for portable electronic equipment and electric vehicles.[1−3] However, the maximum energy density for lithium-ion batteries is around 350 Wh kg^{-1} due to the limited number of active crystallographic sites in the intercalation-based electrode materials, which cannot meet future demands for energy-storage devices. Indeed, energy densities of over 500 Wh kg^{-1} are projected for next-generation batteries, which has prompted an intensive exploration of new battery materials.[4−6] Lithium−sulfur (Li−S) batteries, as a representative of the emerging battery system, have garnered widespread attention in recent years due to the very high theoretical energy density of 2600 Wh kg^{-1} and environmental friendliness.[7] However, as for a Li-ion, the relative scarcity and uneven global distribution of lithium resources is inevitable, a practical problem for Li−S batteries.[8−10]

To overcome issues related to the availability of lithium resources, one promising strategy is to replace lithium with potassium since the potassium reserve in the Earth's crust (2.09 wt %) is much higher than that of lithium (0.0017 wt %).[11−13] Meanwhile, the redox potential of K/K$^+$ (−2.93 V vs. standard hydrogen electrode (SHE)), as compared with the redox potential of Na/Na$^+$ (−2.70 V vs SHE), is closer to that of Li/Li$^+$ (−3.04 V vs SHE) in nonaqueous electrolyte systems.[10,14,15] Moreover, compared with sodium and lithium ions, potassium ions also have advantages in terms of ion conductivity and diffusion kinetics due to their low desolvation energy.[16,17] Benefiting from these advantages, Wang et al. reported that a potassium ion hybrid capacitor, employing phosphorus and oxygen dual-doped porous carbon spheres as anode, can even maintain a capacity retention rate of 89.8% after 10000 ultralong cycles at 20 A g^{-1}.[18] Keeping this in mind, it is obvious that there is a strong driving force to
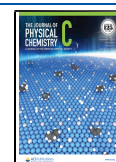
develop K−S batteries by replacing lithium with potassium. However, as is the case for Li−S, K−S batteries suffer from the so-called shuttle effect of soluble polysulfide intermediates, leading to poor Coulombic efficiency and rapid capacity decay upon cycling.[19,20] To mitigate these issues, sulfur is generally embedded in carbon-based materials to inhibit the diffusion of polysulfide species from the cathode into the electrolyte by physical confinement and chemical interactions. Nevertheless, it is not feasible to completely eliminate the shuttle effect.[21,22] Since the radius of the potassium ion (0.138 nm) is much larger than that of the lithium-ion (0.076 nm), K−S batteries will still suffer a rapid decline in capacity with carbon-based cathodes owing to enhanced volume expansion during the charge and discharge processes.[13] Of course, other novel methods have also been tried, such as employing the β''-Al$_2$O$_3$ solid electrolyte to inhibit the shuttle effect or using a potassium-impregnated hard carbon anode in connection with a potassium polysulfide catholyte to realize high-safety K−S batteries.[23,24] Nevertheless, some inherent flaws of these materials hinder their further applications (e.g., high operating temperature and limited cycle stability).

One promising strategy is to change the storage form of sulfur in the active material by chemical interactions.[6] In particular, organic sulfur compounds composed of organic units and sulfur chains can highly and uniformly load abundant sulfur atoms by forming covalent bonds between the organic skeleton and bespoke sulfur chains, which not only avoid sulfur agglomeration, but can also greatly inhibit the diffusion of polysulfide.[25,26] Another advantage of organic sulfur compounds derives from their flexible chains, which are beneficial for alleviating the pulverization of electrode materials caused by volume expansion. As an example of a representative organic sulfur compound, sulfur/polyacrylonitrile (PAN) can be prepared by pyrolyzing PAN with sulfur and used as cathode materials in K−S batteries.[27,28] Due to the absence of long-chain potassium polysulfides (K$_2$S$_n$, n > 3) during the charge and discharge processes, the sulfur/PAN cathodes can largely avoid severe pulverization and prevent the serious capacity decline caused by the dissolution of potassium polysulfide into the electrolyte. Nevertheless, despite the aforementioned advantages, sulfur/PAN materials have an intrinsic limit of low sulfur content (~40 wt %), which is far less than the minimum sulfur content (70 wt %) required to build a high energy density battery.[1,29,30] Meanwhile, the voltage plateaus for sulfur/PAN cathodes are limited within a narrow region due to the absence of high-order potassium polysulfides, which also further reduces the energy density of K−S batteries and blocks their practical applications. Ultimately, the poor K−S properties for sulfur/PAN materials originate from two aspects: (1) a large proportion of the materials is in essence electrochemically inert parts and (2) a limited sulfur chain length. One effective approach to overcome these drawbacks is to introduce long sulfur chains into a covalent framework through inverse vulcanization.[6] In 2013, Pyun's group reported an inverse vulcanization method to obtain poly(sulfur-random-1,3-diisopropenylbenzene) with a staggering sulfur content of 90 wt %, which exhibited an initial specific discharge capacity of 1100 mAh g^{-1} and high capacity retention as an electrode for Li−S batteries.[26] Following this, a series of sulfur copolymers with high sulfur contents (e.g., sulfur-divinylbenzene copolymers,[31] sulfur-trithiocyanuric acid copolymers,[32] sulfur-polyaniline copolymers[33]) were developed and displayed high energy densities as

electrodes for Li−S batteries. However, corresponding studies on K−S batteries are yet to emerge and need to be addressed.

In this work, three comonomers with different numbers of allyloxy linkers (comonomer/linker groups = 1:1, 1:2, and 1:4) are investigated; they are then cross-linked with sulfur to form the sulfur-linked polymers: sulfur-linked 2-allyloxy-naphthoquinone polymer (poly(S1-ANQ)), sulfur-linked 1,4-bis-(allyloxy)-anthraquinone polymer (poly(S2-BAAQ)), and sulfur-linked tetra(allyloxy)-1,4-benzoquinone polymer (poly-(S4-TABQ)). Computational simulations indicate that the strong interaction between allyloxy linkers and potassium polysulfides greatly mitigates the shuttle effect in K−S cells, resulting in the excellent cycling performance. Meanwhile, density functional theory calculations further demonstrate that the bandgap energy of sulfur-linked polymers would dramatically decrease by increasing the number of allyloxy linkers, which will promote the charge transfer in K−S cells and increase the capacity. Owing to the abundant allyloxy linkers in poly(S4-TABQ), resulting in a high sulfur content of ~71 wt %, its corresponding K−S batteries exhibit an excellent cycling stability with a high retention rate of 94.5% after 200 cycles at 0.2 C (0.027% loss cycle^{-1}). Furthermore, the electrochemical mechanism in the poly(S4-TABQ) cathode is investigated by using ex situ X-ray photoelectron spectroscopy and ultraviolet−visible spectroscopy.

2. EXPERIMENTAL SECTION

2.1. Materials. Sulfur (≥99.5%), CH$_2$Cl$_2$ (≥99.5%), CS$_2$ (≥99.5%), and anhydrous N,N-dimethylformamide (DMF, ≥99.5%) were purchased from Tianjing Fengchuan Chemical Reagent Technology Co. Ltd. Tetrahydroxy-1,4-quinone hydrate (≥96%, Aladdin), 1,4-dihydroxyanthraquinone (≥98%, Aladdin), 2-hydroxy-1,4-naphthoquinone (≥98%, TCl), allyl bromide (≥99%, Alfa Aesar), KTFSI (≥99.8%, DoDo Chem), tetraethylene glycol dimethyl ether (TEGDME, ≥99%, Roche), and N-methyl-2-pyrrolidinone (NMP, ≥99.5%, Aladdin) were purchased from different companies. All chemicals were used as received.

2.2. Synthesis of TABQ, BAAQ, and ANQ. Tetra-(allyloxy)-1,4-benzoquinone (TABQ) was synthesized according to previous reports.[33] Briefly, tetrahydroxy-1,4-quinone hydrate (1.10 g) was dissolved in anhydrous DMF (20 mL) under N$_2$ atmosphere, and then K$_2$CO$_3$ (3.54 g) in DMF (70 mL) was added into the solution. After stirring for 15 min, allyl bromide (6.19 g) in DMF (10 mL) was added into the mixture slowly. The reaction mixture was heated to 60 °C under reflux and kept for 12 h. Subsequently, the product was cooled down to 0 °C and then filtered to remove the insoluble substance. Besides, the resultant TABQ was obtained by repeated extractions with CH$_2$Cl$_2$ and deionized water. For BAAQ and ANQ, their synthesis processes took a similar approach as TABQ.

2.3. Synthesis of Sulfur-Linked Polymers. Sulfur-rich polymers with different numbers of linker bonds were synthesized via bulk inverse vulcanization. Typically, a certain amount of elemental sulfur is first placed in a 25 mL round-bottom flask and heated to 160 °C under vigorous stirring. When the molten sulfur changes from yellow to orange, the linker molecules in CH$_2$Cl$_2$ were slowly added into the flask by syringe. After reacting for 3 h, the reaction was terminated by quenching into liquid nitrogen. Finally, the product was obtained by washing with CS$_2$ to be colorless.
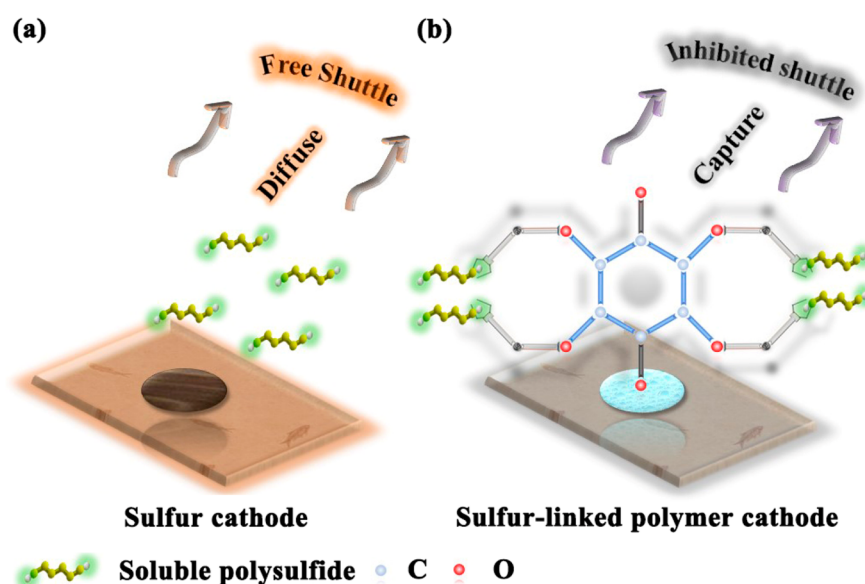
Figure 1. Schematic illustration comparing the ability of (a) sulfur cathode and (b) sulfur-linked polymer (for clarity a monomer unit shown) cathode for mitigating the shuttle effect in K–S batteries.

2.4. Electrochemical Measurements. A mixture of sulfur-linked polymers, polyvinylidene difluoride (PVDF) and Super P in a mass ratio of 60:10:30 were ground in an agate mortar with NMP to form a uniform slurry. As-prepared slurry was coated onto carbon paper with a sulfur loading of 1.0–2.0 mg cm^{-2}, and then vacuum-dried at 40 °C for 24 h. For the preparation of sulfur cathode, a similar procedure was followed. In short, sublimed sulfur, PVDF, and Super P were mixed in a mass ratio of 60:10:30, and then coated on carbon paper resulting in a sulfur loading of 1.0–2.0 mg cm^{-2}. With potassium metal as the counter-electrode and a glass fiber membrane as the separator, CR2032-type coin cells were assembled in an argon-filled glovebox (H$_2$O, O$_2$ < 0.1 ppm). The electrolytes employed were 1 M KTFSI dissolved in TEGDME (60 μL cell^{-1}). The galvanostatic charge/discharge performance (LAND-CT2001A) of the half-cell was tested in a voltage range of 1.2–3.0 V (vs K/K$^+$) at ambient temperature. Cyclic voltammetry (CV) curves were carried out on CHI660E electrochemical test station at a scan rate of 0.1 mV s^{-1} in the range of 1.2–3.0 V. Electrochemical impedance spectra (EIS) were obtained using a PARSTAT MC multichannel electrochemical workstation in the frequency range of 0.01 Hz to 1 MHz with alternating current (AC) amplitude of 10 mV. Specific capacities were calculated on the basis of the mass of sulfur. For the ex situ XPS test, after one precycle at a current of 50 μA, the cells were disassembled after reaching the preset voltage in an argon-filled glovebox. After washing with TEGDME, the cathode was placed in the argon-filled glovebox for 1 h, and then it was sealed with a polyimide film (3 M Company) to isolate the air. For the ex situ UV–vis test, after disassembling the cells, the cathode was immersed in 5 mL of TEGDME and sealed in a cuvette with Ar protection for measurement. The ex situ UV–vis tests were carried out within 20 min to avoid possible side reactions.

2.5. Characterizations. Thermal gravimetric analysis (TGA; NETZSCH STA 2500 simultaneous thermal analyzer) was performed with a heating rate of 10 °C min^{-1} from room temperature to 800 °C under a nitrogen atmosphere. Element analysis (EA) was carried out in a Vario MACRO cube.

Powder X-ray diffraction (XRD) data of sulfur-rich polymers were recorded on a D8 ADVANCE X-ray diffractometer with Cu Ka radiation (λ = 1.5406 Å). X-ray photoelectron spectroscopy (XPS) analyses were performed using a VG ESCALAB 220I-XL device. Ultraviolet–visible spectroscopy (UV-vis; Shimadzu UV-2450 spectrometer) analyses were used to characterize the soluble polysulfide species in TEGDME. The Fourier transform infrared spectroscopy (FT IR; Bruker VERTEX 70v) spectra were recorded using KBr pellets. The transmission electron microscopy (TEM) images were observed by FEI TalosF200S.

2.6. Density Functional Theory (DFT) Calculations. All density functional theory (DFT) calculations were performed in Gaussian 09.[34] The geometry optimization of the three monomers was performed at the PBE1PBE[35]/6-31G(d,p) level with the D3 version of Grimme's dispersion with Becke-Johnson damping.[36] The single-point energy calculation of the optimized structures was performed at the B3LYP/6-31G* level, generating the energies of HOMOs and LUMOs.

2.7. COMSOL Multiphysics Simulations. Based on COMSOL Multiphysics 5.5 software, the "Tertiary current distribution" interface was selected to describe the current and potential distribution in the cell and analyze the transport of polysulfide in the electrolyte. The Butler–Volmer expression was used to reveal the electrode kinetics of the charge transfer reaction at room temperature in the bulk electrolyte. According to previous reports in Li–S batteries,[37,38] a 2D K–S battery model was established after ignoring volume expansion due to polysulfide deposition and simplifying the reaction to three stages of K$_2$S$_8$–K$_2$S$_6$–K$_2$S$_3$. Due to the fast kinetics of the potassium anode, it was replaced with an edge of 19 mm when constructing the 2D model. In addition, the separator and cathode were represented by two rectangles with a width of 9 and 100 μm, respectively. The detailed geometric constructions are shown in Figure S7.

3. RESULTS AND DISCUSSION

As shown in Figure 1a, for a typical sulfur cathode, unbonded soluble polysulfides diffuse freely into the electrolyte, causing a
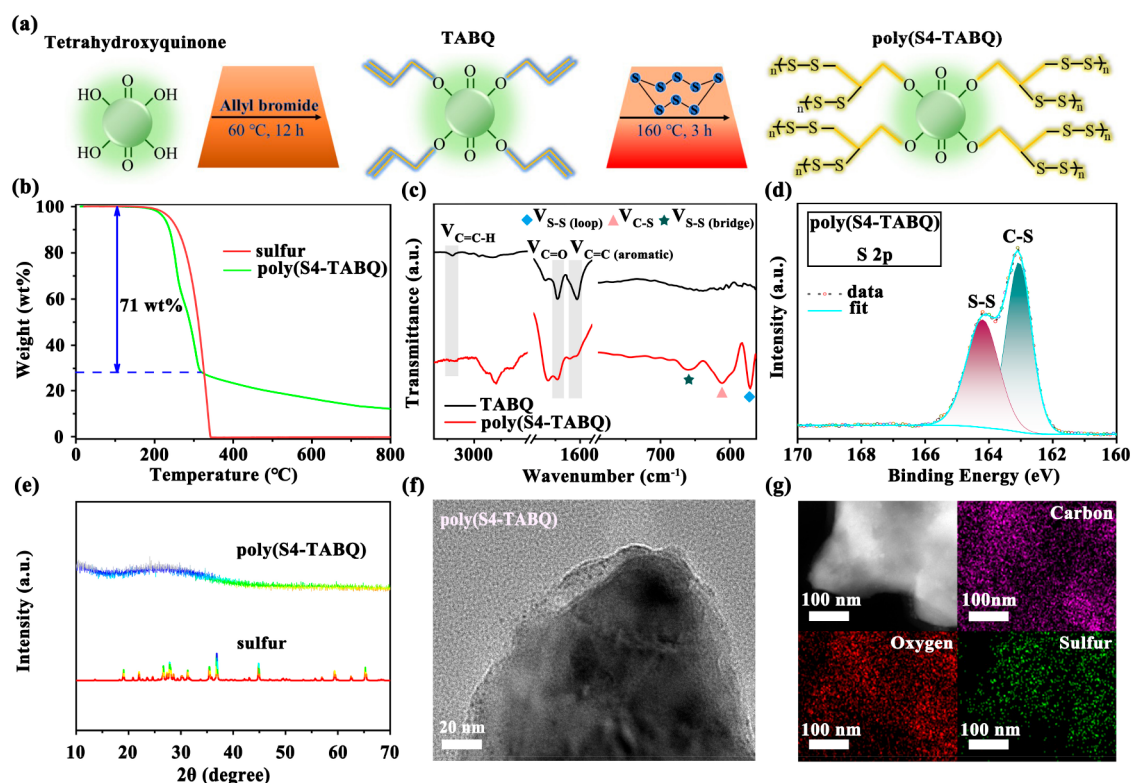
Figure 2. (a) Schematic diagram for the synthesis of poly(S4-TABQ). (b) TGA curves of poly(S4-TABQ), compared with sulfur. (c) FT IR spectra for poly(S4-TABQ) and TABQ. (d) High-resolution XPS spectrum of S 2p for poly(S4-TABQ). (e) XRD patterns of poly(S4-TABQ) and sulfur. (f) TEM image and (g) corresponding elemental mappings (carbon, oxygen and sulfur) of poly(S4-TABQ).

severe shuttle effect in potassium−sulfur (K−S) batteries. This not only leads to a large loss of active material but also a rapid decline in battery capacity. In contrast, when sulfur-linked polymers are employed as cathodes (Figure 1b), soluble polysulfide can be firmly anchored in the polymer cathode through chemical bonds, thereby greatly mitigating the polysulfide shuttle process and achieving high performance. Typical sulfur-linked tetra(allyloxy)-1,4-benzoquinone polymer (poly(S4-TABQ)) was prepared and displayed in Figure 2a, with more details in the Experimental Section. Briefly, a Williamson ether reaction was employed to decorate tetrahydroxyquinone with allyl sites at 60 °C for 12 h under continuous nitrogen gas flow; the product was then mixed with sulfur at 160 °C for 3 h to form a sulfur-linked polymer denoted as poly(S4-TABQ). For the further preparation of sulfur-linked polymers, similar methods are used for sulfur-linked 2-allyloxy-naphthoquinone polymer (denoted as poly-(S1-ANQ)) and sulfur-linked 1,4-bis(allyloxy)-anthraquinone polymer (denoted as poly(S2-BAAQ)). Their chemical structures are shown in Figure S1. The content of sulfur for poly(S4-TABQ) is confirmed to be ∼71 wt % by thermal gravimetric analysis (TGA), as shown in Figure 2b. In the temperature range of 200−280 °C, the weight loss of poly(S4-TABQ) can be attributed to the decomposition of S−S bonds, while the slight weight loss between 280 to 320 °C originates from the C−S bond breaks.[33] Additionally, the step-down decreases of sulfur contents for both poly(S1-ANQ) (∼46 wt %, Figure S2a) and poly(S2-BAAQ) (∼60 wt %, Figure S2b) are due to the reduced number of sites in their corresponding monomer molecules for effective chemical connections with sulfur chains. Meanwhile, elemental analysis (EA) measurements were also used to determine the sulfur contents in the

various sulfur-linked polymers, which are in good agreement with the TGA results (Table S1).

Fourier transform infrared spectroscopy (FT IR) was further used to elucidate the chemical structure of the targeted polymers. As shown in Figure 2c, the vinylic C−H, C=O group, and aromatic C=C bond appear at 3080, 1692, and 1611 cm^{-1}, respectively, demonstrating the successful synthesis of TABQ. However, for poly(S4-TABQ), the vinylic C−H almost disappears because of the addition reaction of allyloxy with sulfur. The C=O group and aromatic C=C bond are still present in poly(S4-TABQ), indicating that the structure of TABQ comonomer is intact after polymerization. Besides, three new peaks appear in poly(S4-TABQ) at 659, 611, and 570 cm^{-1}, respectively, which are attributed to the sulfide loop, C−S bond, and sulfide bridge, respectively. Similarly, the FT IR spectra of poly(S1-ANQ) and poly(S2-BAAQ) are shown in Figure S3. X-ray photoelectron spectroscopy (XPS) was also performed to reveal the chemical state of sulfur groups in the various polymers. Representative results obtained from poly-(S4-TABQ) are shown in Figure 2d, and the XPS results for poly(S1-ANQ) and poly(S2-BAAQ) are shown in Figures S4 and S5 (Supporting Information). The S 2p spectra of poly(S4-TABQ) is shown in Figure 2d; two characteristic peaks indexed at 163.0 and 164.2 eV with an energy separation of 1.2 eV can be attributed to the spin−orbit coupling of S $2p_{3/2}$ and S $2p_{1/2}$, respectively, which indicate the formation of C−S and S−S bonds in poly(S4-TABQ).[21] Besides, the C 1s spectrum of poly(S4-TABQ) at 282.4−290.9 eV can be deconvoluted into C=O, C−O, C−S, and C−C bonds, which further confirms that the molecular structure of TABQ monomer remains intact after the vulcanization reaction (Figure S4c). The combined results of XPS and FT IR
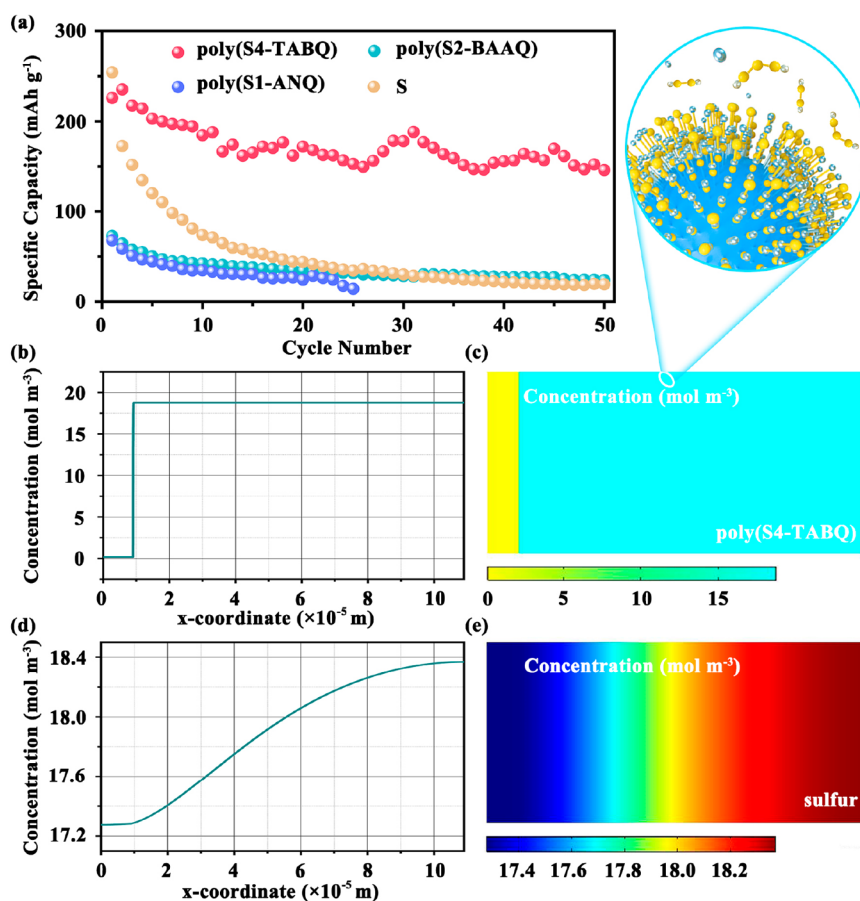
Figure 3. (a) Cycle performance of poly(S4-TABQ), poly(S2-BAAQ), poly(S1-ANQ), and sulfur at 0.1 C. (b) The concentration distribution curve of K_2S_8 (the x-coordinate from 0 to 1×10^{-5} m represents the separator, and from 1 to 11×10^{-5} m represents the cathode) in a K−S cell based on poly(S4-TABQ) as cathode material. (c) The corresponding two-dimensional distribution of K_2S_8 and a cartoon picture showing the strong interaction between the poly(S4-TABQ) and KSBs. (d) The concentration distribution curve of K_2S_8, and (e) the corresponding two-dimensional distribution of K_2S_8 in a K−S cell by using sulfur as a cathode.

demonstrate that sulfur is well cross-linked with TABQ to form sulfur-linked poly(S4-TABQ). X-ray diffraction (XRD) and transmission electron microscopy (TEM) measurements were further performed to confirm the absence of elemental sulfur in the polymers after the inverse vulcanization reaction. As seen in the XRD patterns (Figure 2e), elemental sulfur exhibits strong crystalline peaks, while the poly(S4-TABQ) polymer is free of any peaks except a large broad peak from 15° to 41°. This indicates that sulfur molecules are completely converted to form amorphous polymers, which is in accordance with the goal of covalently combining sulfur atoms with organic skeletons to avoid sulfur agglomeration and inhibit the diffusion of polysulfide. The same is found for poly(S1-ANQ) and poly(S2-BAAQ) (Figure S6). Moreover, the absence of sulfur crystalline phases in the TEM image of poly(S4-TABQ) endorses this finding (Figure 2f). The elemental mapping of poly(S4-TABQ) reveals a homogeneous distribution of C, O, and S elements (Figure 2g).

To gain insight into the electrochemical performance of various organosulfur cathodes, K−S cells were fabricated with K metal as the counter-electrode and 1 M potassium bis(trifluoromethylsulfonyl)imide (KTFSI) in tetraethylene glycol dimethyl ether (TEGDME) as the electrolyte. Figure 3a displays the electrochemical performances of polymer cathodes with various numbers of allyloxy linkers, which are

operated at 0.1 C (1 C = 1675 mAh g^{-1}). Compared with poly(S1-ANQ) and poly(S2-BAAQ) cathodes, it is clear that the poly(S4-TABQ) cathode exhibits vastly superior energy storage performance. Although the sulfur cathode has a high initial capacity of 254.2 mAh g^{-1}, the severe shuttle effect of the sulfur cathode leads to a rapid capacity decay of 92.4% after 50 cycles. As can be seen, the capacity decline could be greatly alleviated by introducing allyl sites. In particular, the poly(S4-TABQ) cathode delivers not only a much higher initial specific capacity (225.9 mAh g^{-1}) when compared to other organo-sulfur polymer-based cathodes of poly(S1-ANQ) (68 mAh g^{-1}) and poly(S2-BAAQ) (72.8 mAh g^{-1}), but also an improved and well-maintained capacity of 64.6% after 50 cycles. In order to reveal the structural advantages of organosulfur polymer-based cathodes, a 2D battery model (detailed geometric construction is shown in Figure S7) was constructed using COMSOL Multiphysics to simulate the diffusion of polysulfide during discharging. As shown in Figure 3b, depending on the strong interaction between poly(S4-TABQ) and potassium polysulfide (KSBs), KSBs are still firmly confined to the cathode, even at a high concentration of 19 mol m^{-3}, and the concentration of KSBs is almost zero outside the cathode area (separator area). Meanwhile, the colors, where the cyan and yellow parts represent high and low concentrations of KSBs, respectively, are completely different

between the separation and the cathode areas, demonstrating that the shuttle effect in the poly(S4-TABQ) cathode is significantly suppressed (Figure 3c). In contrast, the KSBs present a free diffusion in a K−S battery by using sulfur cathode, and its concentration near the anode is as high as 17.3 mol m^{-3}, which will lead to serious side effects in battery operation, for example, resulting in a fast capacity decline (Figure 3d,e). Thus, as shown in Figure 3c, owing to the introduction of functionally linked groups, KSBs are firmly fixed to poly(S4-TABQ) cathode during the discharge process with no obvious sign of the shuttle effect, thereby realizing the high battery stability.

Although the simulation indicates that the allyloxy linkers in sulfur-linked polymer cathodes have a positive effect on the cycling stability of K−S batteries, the reason why an increasing number of allyloxy linkers is beneficial for achieving higher capacity is unclear. Therefore, further analysis using density functional theory (DFT) was performed. The energy levels of the HOMO and LUMO positions for the different monomers of poly(S1-ANQ), poly(S2-BAAQ), and poly(S4-TABQ) were calculated and shown in Figure 4. It is interesting that the
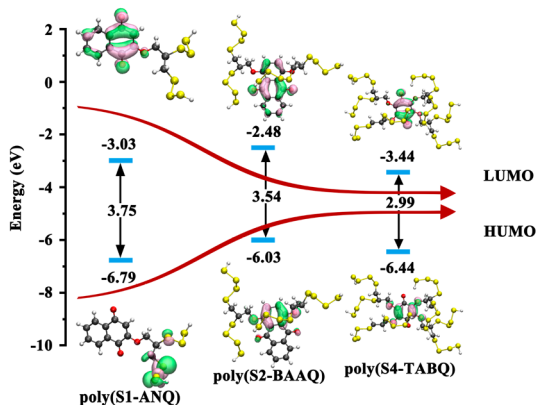

Figure 4. Molecular orbital diagram of the evaluated HOMO and LUMO levels of poly(S1-ANQ), poly(S2-BAAQ), and poly(S4-TABQ).

bandgap of sulfur-linked polymers is strongly related to the number of allyloxy linker groups: the larger the number is, the narrower the bandgap becomes. For example, the poly(S4-TABQ) has the narrowest bandgap of 2.99 eV when compared with the other two polymers. It should be noted that low bandgap energy is beneficial for electron transfer in the polymer, which can improve electrical conductivity, leading to increased capacity.[39] Here, the allyl linker may act as a "bridge" between KSBs and the polymers. Not only does it promote the redox reaction of KSBs, but it also improves the utilization rate of active species. Therefore, compared with the other two polymers, poly(S4-TABQ) shows the highest capacity. Such a phenomenon has also been found in lithium−sulfur (Li−S) batteries, but the implication of this does not appear to have been fully appreciated.[40,41] For example, 1,3-diisopropenyl-benzene (DIB) is known as the most widely employed sulfur-linker polymer, however, when the number of isoprene linkers in DIB is reduced, both the stability and capacity of the battery fall sharply.[40,41] Overall, these results suggest that the construction of polymers with low band gap energy is possible by simply adding a linker. This is also an effective way for preparing an advanced K−S battery owing to the "bridge"

effect of the linker. Clearly, the DFT calculations provide an explanation for the relationship between the molecular structure of the sulfur-linked polymer and the electrochemical capacity for K−S batteries.

To evaluate the potential for poly(S4-TABQ) in practical applications, the electrochemical properties were examined. As shown in Figure 5a, the discharge capacity of the poly(S4-TABQ) cathode is 189.3 mAh g^{-1} at 0.1 C, which can be preserved as 100%, 82.5%, 44.8%, 23.2%, and 11.8% at C-rates of 0.1, 0.2, 0.5, 1, and 2 C, respectively. When the C-rate switches back to 0.1 C, the K−S cell with poly(S4-TABQ) cathode still delivers a capacity of 186.4 mAh g^{-1}, demonstrating the excellent rate capability of poly(S4-TABQ). By stark contrast, the rate properties of the sulfur cathode, the poly(S1-ANQ) cathode, and the poly(S2-BAAQ) cathode are inferior, among which the sulfur cathode is the worst one with a rapid capacity decline due to its severe shuttle effect (Figure S8). Moreover, the electrochemical impedance spectroscopy (EIS) analysis (Figure 5b) shows that the charge-transfer resistance (R_{ct}) of the poly(S4-TABQ) cathode drastically reduces from 2719 to 180 Ω after 10 cycles, which is further reduced to 107 Ω after another 40 cycles. This observation may result from the formation of a stable interface between the electrode and the electrolyte during cycling.[18] Meanwhile, even when the 100th cycle is reached, the impedance value has hardly changed; this can be attributed to the excellent structural stability of poly(S4-TABQ). The charge−discharge voltage profiles in Figure 5c show the excellent stability of poly(S4-TABQ), corresponding to a capacity retention of 96.1% after 100 cycles at 0.2 C. Moreover, owing to the low bandgap energy of 2.99 eV, the polarization degree of poly(S4-TABQ) increased slightly (∼6 mV) after 100 cycles. Figure 5d shows the cyclic voltammetry (CV) curves for the poly(S4-TABQ) cathode from 1.2 to 3.0 V with a scan rate of 0.1 mV s^{-1}. Three wide peaks appear at B1 (∼1.6 V), B2 (∼2.0 V), and B3 (∼2.5 V) during the discharge process, which can be attributed to the different reactions between the sulfur and potassium ions. Specifically, the peaks at B2 and B3 are related to the stepwise reduction to long-chain polysulfides (S_6^{2-}, S_5^{2-}), while another peak at B1 is associated with the formation of short-chain sulfides (S_3^{2-}, S_2^{2-}).[11,12,42] In addition, two anodic peaks appear at A1 (∼2.2 V) and A2 (∼2.8 V), which are related to a reversible oxidation process. The asymmetric paths between charge and discharge may indicate that some reactions occur,[12] as seen as well for the sulfur cathode (Figure S9a). The sulfur cathode exhibits chaotic CV curves due to the severe shuttle effect, while the CV curves of the poly(S1-ANQ) cathode show a slightly irreversible feature (Figure S9b). Furthermore, owing to the presence of additional allyloxy linkers in poly(S2-BAAQ), the CV curves of the poly(S2-BAAQ) cathode show a relatively better stability than those of poly(S1-ANQ) (Figure S9c). Nevertheless, the redox activity of poly(S2-BAAQ) is still limited when compared with that of poly(S4-TABQ) due to the higher bandgap energy of poly(S2-BAAQ). As plotted in Figure 5e, the long-term cycling stability of the poly(S4-TABQ) cathode was also studied at 0.2 C for 200 cycles. As expected, the performance of the sulfur cathode is extremely poor, with almost no capacity after only 100 cycles; this implies that the shuttle effect is catastrophic for the performance of K−S batteries. Thus, high capacity retention is very difficult to realize in K−S batteries when the sulfur content in the cathode is as high as 71 wt %. However, the poly(S4-TABQ) cathode
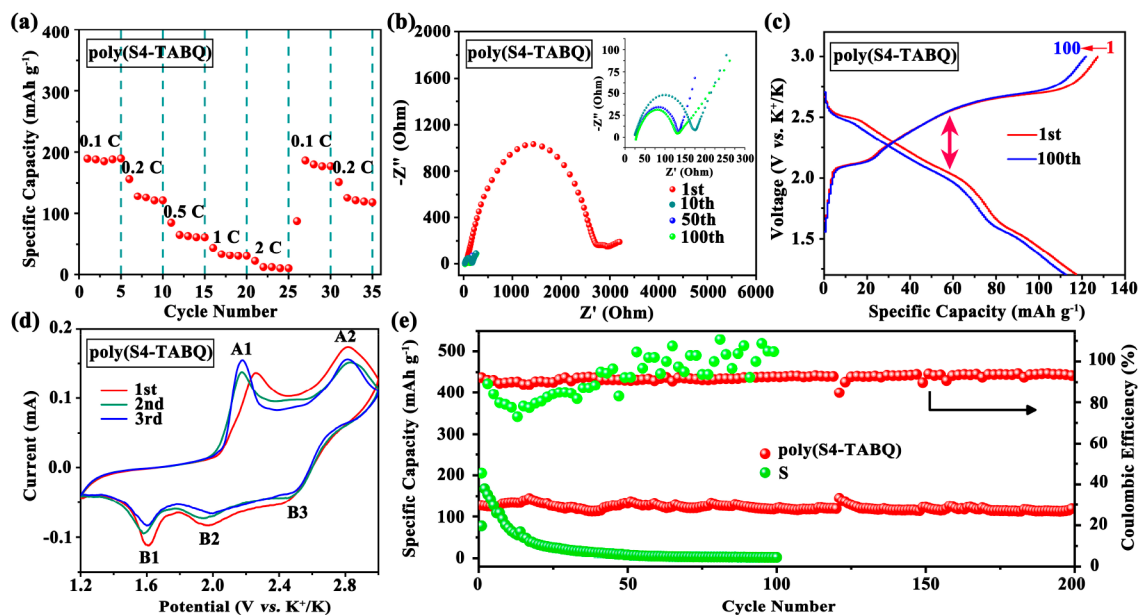
Figure 5. (a) Rate capability test of a potassium−sulfur cell based on a poly(S4-TABQ) cathode. (b) EIS measurements of poly(S4-TABQ) cathode at the 1st, 10th, 50th, and 100th cycles, respectively. (c) Galvanostatic discharge/charge voltage profiles of poly(S4-TABQ) cathode at the 1st and 100th cycle(s). (d) CV curves of the poly(S4-TABQ) cathode with a scan rate of 0.1 mV s^{-1}. (e) Long-term cycle performance of potassium−sulfur cells based on poly(S4-TABQ) and sulfur cathode at 0.2 C.
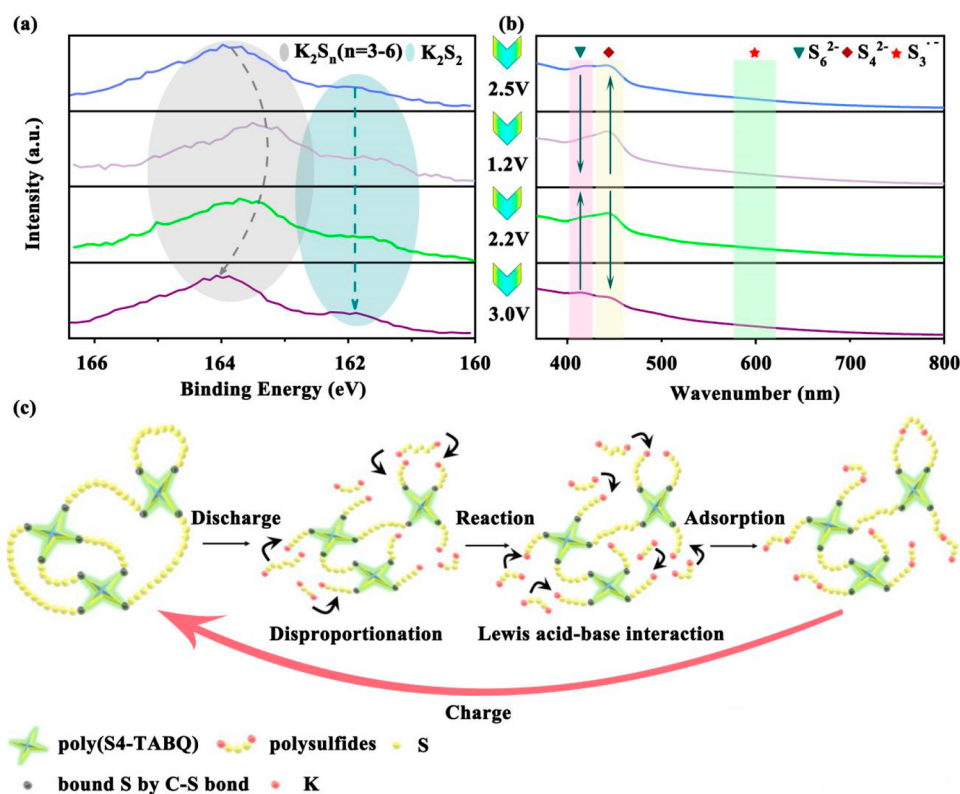
Figure 6. (a) Ex situ XPS data of S 2p with a poly(S4-TABQ) cathode at preset voltage plateaus in a K−S cell. (b) Ex situ UV−vis analysis of poly(S4-TABQ) electrode at different voltage plateaus. (c) Schematic representation of the reaction mechanisms during the discharge and charge process in a K−S cell.

exhibits a high reversible specific capacity of 119 mAh g^{-1} after 200 cycles at 0.2 C, corresponding to a capacity retention of 94.5% (0.027% loss per cycle). Such an excellent performance of the poly(S4-TABQ) may be attributed to the allyloxy linker

effect and low band gap energy; this approach could therefore be a route to realize high-performance K−S batteries.

To further study the underlying electrochemical mechanism of the poly(S4-TABQ) cathode during the charge and

discharge processes, a series of advanced characterizations were conducted, including ex situ XPS and ultraviolet−visible spectroscopy (UV−vis) methods. As shown in the XPS spectra in Figure 6a, two main peaks at around 161.9 and 162.5−165.9 eV are observed under different voltages, corresponding to the K_2S_2 and K_2S_n ($n = 3−6$) species, respectively.[26,43−45] The absence of the peaks between 160 and 161 eV indicates that K_2S has not been formed during the electrochemical process. This may be because the K_2S group (Gibbs Energy of Formation at 25 °C, $\Delta G_f^0 = −410$ kJ mol^{-1}) is much more unstable compared to the K_2S_3 group ($\Delta G_f^0 = −528$ kJ mol^{-1}) from a thermodynamic perspective.[46] Meanwhile, the sluggish reduction kinetics of the insoluble K_2S_3 further hinders its transfer into K_2S.[12,23,46] Besides, during the discharge process, the peaks at 162.5−165.9 eV, which are related to K_2S_n ($n = 3−6$), gradually shift to lower binding energy, while the phenomenon is reversed after charging. This can be attributed to the conversion of long-chain polysulfide ($n = 5−6$) to short-chain polysulfide ($n = 3−4$).[42,47] Ex situ UV−vis further elucidates the electrochemical mechanism in the cell. As Figure 6b shows, the S_4^{2-}, S_6^{2-}, and $S_3^{·-}$ groups are dominant in the solution.[11,48−50] The broad peak at ∼414 nm (associated with S_6^{2-}) disappears when discharged to 1.2 V, while gradually recovering after charging. However, the trend for the S_4^{2-} group is the opposite. These results are consistent with the XPS analysis discussed earlier. In addition, the presence of the $S_3^{·-}$ free radical in the cathode provides additional chemical pathways, which can also promote the disproportionation reaction, thereby mitigating the shuttle effect.[48]

Based on these new insights combined with related previous reports,[41,42] the reaction mechanism of sulfur-linked polymer cathodes in the K-system is likely described by general eq 1.

$$-C-S_n-C-+3K^+ \underset{\text{charge}}{\overset{\text{discharge}}{\rightleftarrows}} -C-S_n^-\cdot K^+(n=2-6)$$
$$+ K_2S_n(n=2-6) \qquad (1)$$
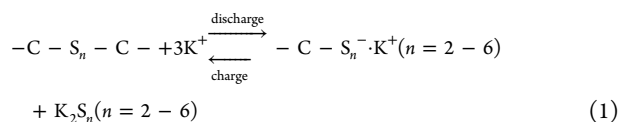
It is worth noting that organic and inorganic polysulfides coexist in the poly(S4-TABQ) cathode. The S−S bonds in the polymer will be broken to form $-C-S_n^-\cdot K^+$ ($n = 2−6$) and inorganic K_2S_n during the discharge process, which is similar to the SPAN cathode.[51] As plotted in Figure 6c, with both organic and inorganic KSBs formation simultaneous, species could combine through Lewis acid−base interactions or a disproportionation reaction, which greatly inhibit the polysulfide shuttling and endow the K−S battery with excellent cyclic stability. After charging, the S−S bonds will return to the long-chain state, resulting in a reversible cycle process. Thus, in the design of sulfur-linked polymer cathodes, for achieving high-performance K−S batteries, it is critical that sufficient functional linkers are present at all times.

4. CONCLUSIONS

In summary, it has been demonstrated that by introducing abundant allyloxy linkers, the poly(S4-TABQ) polymer-based cathode exhibits high cyclic stability (0.027% loss cycle^{-1}) even with high sulfur content (∼71 wt %) due to fast charge transfer properties and a strong interaction with potassium polysulfide. This finding provides design principles for next-generation sulfur-linked polymer cathodes in even higher-performance K−S batteries. The two key principles are (1) the introduction of abundant linkers to ensure strong interaction between the electrode materials and potassium polysulfides,

which will greatly limit the shuttle effect and (2) low bandgap energy of sulfur-linked polymers can be achieved by adjusting the number and structure of linkers to ensure fast charge transfer. Furthermore, spectroscopic analysis has proven that the electrochemical mechanism of sulfur-rich polymer cathodes is related to the formation of $-C-S_n^-K^+$ ($n = 2−6$) and K_2S_n ($n = 2−6$) during the charge and discharge processes. Besides, K_2S_2 has also been demonstrated in potassium−sulfur cells, indicating that appropriate catalysts in such electrode materials are necessary to reduce polarization and promote the formation of K_2S to maximize the energy density. Overall, this work demonstrates the potential of generating sulfur-rich polymer cathodes for applications in high-performance potassium−sulfur batteries.

■ ASSOCIATED CONTENT

ⓈＩ Supporting Information

The Supporting Information is available free of charge at https://pubs.acs.org/doi/10.1021/acs.jpcc.1c05283.

The chemical structures of poly(S1-ANQ) and poly(S2-BAAQ), TGA curves determination of sulfur content in poly(S1-ANQ) and poly(S2-BAAQ), the analysis of polymer structures by FT IR and XRS, tests for the presence of sulfur, the existing form of sulfur in polymers by XRD, the geometric domain constructions in COMSOL Multiphysics simulation, the rate performance and CV tests of sulfur, poly(S1-ANQ) and poly(S2-BAAQ) cathodes, sulfur content analysis for poly(S1-ANQ) and poly(S2-BAAQ) by EA measurements, and comparison of relative literature values with this work (PDF)

■ AUTHOR INFORMATION

Corresponding Authors

Jiajia Huang − *School of Chemical Engineering, Zhengzhou University, Zhengzhou 450001, People's Republic of China*; Email: huangjiajia@zzu.edu.cn

Feili Lai − *Department of Chemistry, KU Leuven, Leuven 3001, Belgium*; ⓞ orcid.org/0000-0002-4945-0737; Email: feili.lai@kuleuven.be

Authors

Leiqian Zhang − *School of Chemical Engineering, Zhengzhou University, Zhengzhou 450001, People's Republic of China*

Lingfeng Ge − *School of Chemistry, University of Bristol, Bristol BS8 1TS, United Kingdom*

Guanjie He − *Electrochemical Innovation Lab (EIL), Department of Chemical Engineering, University College London (UCL), London WC1E 7JE, United Kingdom*; ⓞ orcid.org/0000-0002-7365-9645

Zhihong Tian − *School of Chemical Engineering, Zhengzhou University, Zhengzhou 450001, People's Republic of China*

Jingtao Wang − *School of Chemical Engineering, Zhengzhou University, Zhengzhou 450001, People's Republic of China*; ⓞ orcid.org/0000-0002-2004-9640

Dan J.L. Brett − *Electrochemical Innovation Lab (EIL), Department of Chemical Engineering, University College London (UCL), London WC1E 7JE, United Kingdom*; ⓞ orcid.org/0000-0002-8545-3126

Johan Hofkens − *Department of Chemistry, KU Leuven, Leuven 3001, Belgium; Max Planck Institute for Polymer*

Research, Mainz 55128, Germany; ● orcid.org/0000-0002-9101-0567

Tianxi Liu − *Key Laboratory of Synthetic and Biological Colloids, Ministry of Education, School of Chemical and Material Engineering, Jiangnan University, Wuxi 214122, People's Republic of China*

Complete contact information is available at:
https://pubs.acs.org/10.1021/acs.jpcc.1c05283

Notes
The authors declare no competing financial interest.

■ REFERENCES

(1) Chung, S.-H.; Manthiram, A. Current Status and Future Prospects of Metal-Sulfur Batteries. *Adv. Mater.* **2019**, *31*, 1901125.

(2) Li, W.; Song, B.; Manthiram, A. High-Voltage Positive Electrode Materials for Lithium-ion Batteries. *Chem. Soc. Rev.* **2017**, *46*, 3006−3059.

(3) Amine, K.; Belharouak, I.; Chen, Z.; Tran, T.; Yumoto, H.; Ota, N.; Myung, S.-T.; Sun, Y.-K. Nanostructured Anode Material for High-Power Battery System in Electric Vehicles. *Adv. Mater.* **2010**, *22*, 3052−3057.

(4) Zhang, X.; Chen, K.; Sun, Z.; Hu, G.; Xiao, R.; Cheng, H.-M.; Li, F. Structure-Related Electrochemical Performance of Organosulfur Compounds for Lithium-Sulfur Batteries. *Energy Environ. Sci.* **2020**, *13*, 1076−1095.

(5) Liu, Y.; Zhu, Y.; Cui, Y. Challenges and Opportunities towards Fast-Charging Battery Materials. *Nat. Energy* **2019**, *4*, 540−550.

(6) Fang, R.; Xu, J.; Wang, D.-W. Covalent Fixing of Sulfur in Metal-Sulfur Batteries. *Energy Environ. Sci.* **2020**, *13*, 432−471.

(7) Zhao, F.; Li, Y.; Feng, W. Recent Advances in Applying Vulcanization/Inverse Vulcanization Methods to Achieve High-Performance Sulfur-Containing Polymer Cathode Materials for Li-S Batteries. *Small Methods* **2018**, *2*, 1800156.

(8) Lei, K.; Li, F.; Mu, C.; Wang, J.; Zhao, Q.; Chen, C.; Chen, J. High K-Storage Performance Based on the Synergy of Dipotassium Terephthalate and Ether-Based Electrolytes. *Energy Environ. Sci.* **2017**, *10*, 552−557.

(9) Tian, Z.; Chui, N.; Lian, R.; Yang, Q.; Wang, W.; Yang, C.; Rao, D.; Huang, J.; Zhang, Y.; Lai, F.; Liu, C.; Liu, T. Dual anionic vacancies on carbon nanofiber threaded MoSSe arrays: A free-standing anode for high-performance potassium-ion storage. *Energy Storage Mater.* **2020**, *27*, 591−598.

(10) Liang, Y.; Luo, C.; Wang, F.; Hou, S.; Liou, S.-C.; Qing, T.; Li, Q.; Zheng, J.; Cui, C.; Wang, C. An Organic Anode for High Temperature Potassium-Ion Batteries. *Adv. Energy Mater.* **2019**, *9*, 1802986.

(11) Wang, L.; Bao, J.; Liu, Q.; Sun, C.-F. Concentrated Electrolytes Unlock the Full Energy Potential of Potassium-Sulfur Battery Chemistry. *Energy Storage Mater.* **2019**, *18*, 470−475.

(12) Gu, S.; Xiao, N.; Wu, F.; Bai, Y.; Wu, C.; Wu, Y. Chemical Synthesis of K_2S_2 and K_2S_3 for Probing Electrochemical Mechanisms in K-S Batteries. *ACS Energy Lett.* **2018**, *3*, 2858−2864.

(13) Ding, J.; Zhang, H.; Fan, W.; Zhong, C.; Hu, W.; Mitlin, D. Review of Emerging Potassium-Sulfur Batteries. *Adv. Mater.* **2020**, *32*, 1908007.

(14) Zong, W.; Yang, C.; Mo, L.; Ouyang, Y.; Guo, H.; Ge, L.; Miao, Y.; Rao, D.; Zhang, J.; Lai, F.; Liu, T. Elucidating Dual-Defect Mechanism in Rhenium Disulfide Nanosheets with Multi-dimensional Ion Transport Channels for Ultrafast Sodium Storage. *Nano Energy* **2020**, *77*, 105189.

(15) Zhao, S.; Guo, Z.; Yan, K.; Guo, X.; Wan, S.; He, F.; Sun, B.; Wang, G. The Rise of Prussian Blue Analogs: Challenges and Opportunities for High-Performance Cathode Materials in Potassium-Ion Batteries. *Small Struct.* **2021**, *2*, 2000054.

(16) Zhao, S.; Dong, L.; Sun, B.; Yan, K.; Zhang, J.; Wan, S.; He, F.; Munroe, P.; Notten, P. H. L.; Wang, G. $K_2Ti_2O_5$@C Microspheres with Enhanced K^+ Intercalation Pseudocapacitance Ensuring Fast Potassium Storage and Long-Term Cycling Stability. *Small* **2020**, *16*, 1906131.

(17) Zhao, S.; Yan, K.; Munroe, P.; Sun, B.; Wang, G. Construction of Hierarchical $K_{1.39}Mn_3O_6$ Spheres via AlF_3 Coating for High-Performance Potassium-Ion Batteries. *Adv. Energy Mater.* **2019**, *9*, 1803757.

(18) Zhao, S.; Yan, K.; Liang, J.; Yuan, Q.; Zhang, J.; Sun, B.; Munroe, P.; Wang, G. Phosphorus and Oxygen Dual-Doped Porous Carbon Spheres with Enhanced Reaction Kinetics as Anode Materials for High-Performance Potassium-Ion Hybrid Capacitors. *Adv. Funct. Mater.* **2021**, *31*, 2102060.

(19) Zhu, X.; Ouyang, Y.; Chen, J.; Zhu, X.; Luo, X.; Lai, F.; Zhang, H.; Miao, Y.-E.; Liu, T. In Situ Extracted Poly(acrylic acid) Contributing to Electrospun Nanofiber Separators with Precisely Tuned Pore Structures for Ultra-stable Lithium-sulfur Batteries. *J. Mater. Chem. A* **2019**, *7*, 3253−3263.

(20) Xiong, P.; Han, X.; Zhao, X.; Bai, P.; Liu, Y.; Sun, J.; Xu, Y. Room-Temperature Potassium-Sulfur Batteries Enabled by Microporous Carbon Stabilized Small-Molecule Sulfur Cathodes. *ACS Nano* **2019**, *13*, 2536−2543.

(21) Yan, J.; Li, B.; Liu, X. Nano-Porous Sulfur-Polyaniline Electrodes for Lithium-Sulfur Batteries. *Nano Energy* **2015**, *18*, 245−252.

(22) Peng, H.-J.; Zhang, Q. Designing Host Materials for Sulfur Cathodes: From Physical Confinement to Surface Chemistry. *Angew. Chem. Int. Ed.* **2015**, *54*, 11018−11020.

(23) Hwang, J.-Y.; Kim, H.-M.; Yoon, C. S.; Sun, Y.-K. Toward High-Safety Potassium-Sulfur Batteries Using a Potassium Polysulfide Catholyte and Metal-Free Anode. *ACS Energy Lett.* **2018**, *3*, 540−541.

(24) Lu, X.; Bowden, M. E.; Sprenkle, V. L.; Liu, J. A Low Cost, High Energy Density, and Long Cycle Life Potassium-Sulfur Battery for Grid-Scale Energy Storage. *Adv. Mater.* **2015**, *27*, 5915−5922.

(25) Zhao, X.; Hong, Y.; Cheng, M.; Wang, S.; Zheng, L.; Wang, J.; Xu, Y. High Performance Potassium-Sulfur Batteries and Their Reaction Mechanism. *J. Mater. Chem. A* **2020**, *8*, 10875−10884.

(26) Chung, W. J.; Griebel, J. J.; Kim, E. T.; Yoon, H.; Simmonds, A. G.; Ji, H. J.; Dirlam, P. T.; Glass, R. S.; Wie, J. J.; Nguyen, N. A.; et al. The Use of Elemental Sulfur as an Alternative Feedstock for Polymeric Materials. *Nat. Chem.* **2013**, *5*, 518−524.

(27) Liu, Y.; Wang, W.; Wang, J.; Zhang, Y.; Zhu, Y.; Chen, Y.; Fu, L.; Wu, Y. Sulfur Nanocomposite as a Positive Electrode Material for Rechargeable Potassium-Sulfur Batteries. *Chem. Commun.* **2018**, *54*, 2288−2291.

(28) Wei, S.; Ma, L.; Hendrickson, K. E.; Tu, Z.; Archer, L. A. Metal-Sulfur Battery Cathodes Based on PAN-Sulfur Composites. *J. Am. Chem. Soc.* **2015**, *137*, 12143−12152.

(29) Abdul Razzaq, A.; Yao, Y.; Shah, R.; Qi, P.; Miao, L.; Chen, M.; Zhao, X.; Peng, Y.; Deng, Z. High-Performance Lithium Sulfur Batteries Enabled by a Synergy between Sulfur and Carbon Nanotubes. *Energy Storage Mater.* **2019**, *16*, 194−202.

(30) Sohn, H.; Gordin, M. L.; Regula, M.; Kim, D. H.; Jung, Y. S.; Song, J.; Wang, D. Porous Spherical Polyacrylonitrile-Carbon Nanocomposite with High Loading of Sulfur for Lithium-Sulfur Batteries. *J. Power Sources* **2016**, *302*, 70−78.

(31) Gomez, I.; Mecerreyes, D.; Blazquez, J. A.; Leonet, O.; Ben Youcef, H.; Li, C.; Gomez-Camer, J. L.; Bondarchuk, O.; Rodriguez-Martinez, L. Inverse Vulcanization of Sulfur with Divinylbenzene: Stable and Easy Processable Cathode Material for Lithium-sulfur Batteries. *J. Power Sources* **2016**, *329*, 72−78.

(32) Zeng, S.; Li, L.; Xie, L.; Zhao, D.; Zhou, N.; Wang, N.; Chen, S. Graphene-Supported Highly Crosslinked Organosulfur Nanoparticles as Cathode Materials for High-Rate, Long-Life Lithium-Sulfur Battery. *Carbon* **2017**, *122*, 106−113.

(33) Kang, H.; Kim, H.; Park, M. J. Sulfur-Rich Polymers with Functional Linkers for High-Capacity and Fast-Charging Lithium-Sulfur Batteries. *Adv. Energy Mater.* **2018**, *8*, 1802423.

(34) Frisch, M. J.; Trucks, G. W.; Schlegel, H. B.; Scuseria, G. E.; Robb, M. A.; Cheeseman, J. R.; Scalmani, G.; Barone, V.; Mennucci, B.; Petersson, G. A. et al. *Gaussian 09*, revision D.01; Gaussian, Inc.: Wallingford, CT, 2013.

(35) Adamo, C.; Barone, V. Toward Reliable Density Functional Methods without Adjustable Parameters: The PBE0Model. *J. Chem. Phys.* **1999**, *110*, 6158−6170.

(36) Grimme, S.; Ehrlich, S.; Goerigk, L. Effect of the Damping Function in Dispersion Corrected Density Functional Theory. *J. Comput. Chem.* **2011**, *32*, 1456−1465.

(37) Kumaresan, K.; Mikhaylik, Y.; White, R. E. A Mathematical Model for a Lithium-Sulfur Cell. *J. Electrochem. Soc.* **2008**, *155*, A576−A582.

(38) Ghaznavi, M.; Chen, P. Sensitivity Analysis of a Mathematical Model of Lithium-Sulfur Cells Part I: Applied Discharge Current and Cathode Conductivity. *J. Power Sources* **2014**, *257*, 394−401.

(39) Zhang, P.; Zhang, D.; Huang, L.; Hui, W.; Wei, Q.; Song, S. First-Principles Study of Electronic Structure of Nb-Doped LiFePO$_4$. *Rare Metal Mater. Eng.* **2013**, *42*, 718−723.

(40) Dai, S.; Feng, Y.; Wang, P.; Wang, H.; Liang, H.; Wang, R.; Linkov, V.; Ji, S. Highly Conductive Copolymer Sulfur Composites with Covalently Grafted Polyaniline for Stable and Durable Lithium-Sulfur Batteries. *Electrochim. Acta* **2019**, *321*, 134678.

(41) Simmonds, A. G.; Griebel, J. J.; Park, J.; Kim, K. R.; Chung, W. J.; Oleshko, V. P.; Kim, J.; Kim, E. T.; Glass, R. S.; Soles, C. L.; Sung, Y. E.; Char, K.; Pyun, J. Inverse Vulcanization of Elemental Sulfur to Prepare Polymeric Electrode Materials for Li-S Batteries. *ACS Macro Lett.* **2014**, *3*, 229−232.

(42) Hoefling, A.; Nguyen, D. T.; Partovi-Azar, P.; Sebastiani, D.; Theato, P.; Song, S.-W.; Lee, Y. J. Mechanism for the Stable Performance of Sulfur-Copolymer Cathode in Lithium-Sulfur Battery Studied by Solid-State NMR Spectroscopy. *Chem. Mater.* **2018**, *30*, 2915−2923.

(43) Yu, X.; Manthiram, A. A Reversible Nonaqueous Room-temperature Potassium-Sulfur Chemistry for Electrochemical Energy Storage. *Energy Storage Mater.* **2018**, *15*, 368−373.

(44) Fantauzzi, M.; Elsener, B.; Atzei, D.; Rigoldi, A.; Rossi, A. Exploiting XPS for the Identification of Sulfides and Polysulfides. *RSC Adv.* **2015**, *5*, 75953−75963.

(45) Smart, R. S. C.; Skinner, W. M.; Gerson, A. R. XPS of Sulphide Mineral Surfaces: Metal-deficient, Polysulphides, Defects and Elemental Sulphur. *Surf. Interface Anal.* **1999**, *28*, 101−105.

(46) Lai, N.; Cong, G.; Lu, Y. A High-Energy Potassium-Sulfur Battery Enabled by Facile and Effective Imidazole-Solvated Copper Catalysts. *J. Mater. Chem. A* **2019**, *7*, 20584−20589.

(47) Yu, X.; Manthiram, A. Na$_2$S-Carbon Nanotube Fabric Electrodes for Room-Temperature Sodium-Sulfur Batteries. *Chem. Eur. J.* **2015**, *21*, 4233−4237.

(48) Cuisinier, M.; Hart, C.; Balasubramanian, M.; Garsuch, A.; Nazar, L. F. Radical or Not Radical: Revisiting Lithium-Sulfur Electrochemistry in Nonaqueous Electrolytes. *Adv. Energy Mater.* **2015**, *5*, 1401801.

(49) Bieker, G.; Wellmann, J.; Kolek, M.; Jalkanen, K.; Winter, M.; Bieker, P. Influence of Cations in Lithium and Magnesium Polysulphide Solutions: Dependence of the Solvent Chemistry. *Phys. Chem. Chem. Phys.* **2017**, *19*, 11152−11162.

(50) Kawase, A.; Shirai, S.; Yamoto, Y.; Arakawa, R.; Takata, T. Electrochemical Reactions of Lithium-Sulfur Batteries: An Analytical Study Using the Organic Conversion Technique. *Phys. Chem. Chem. Phys.* **2014**, *16*, 9344−9350.

(51) Hwang, J.-Y.; Kim, H. M.; Sun, Y.-K. High Performance Potassium-Sulfur Batteries Based on a Sulfurized Polyacrylonitrile Cathode and Polyacrylic Acid Binder. *J. Mater. Chem. A* **2018**, *6*, 14587−14593.